Available online at www.sciencedirect.com

ScienceDirect

Acta Materialia 79 (2014) 258–267

Acta MATERIALIA

www.elsevier.com/locate/actamat

Growth of intermetallic compounds in the Au–In system: Experimental study and 1-D modelling

L. Deillon [a,b,c,*,1], T. Hessler [a], A. Hessler-Wyser [c], M. Rappaz [b]

[a] The Swatch Group R&D S.A., division Asulab, 2074 Marin, Switzerland
[b] Laboratoire de Simulation des Matériaux, École Polytechnique Fédérale de Lausanne, 1015 Lausanne, Switzerland
[c] Centre Interdisciplinaire de Microscopie Électronique, École Polytechnique Fédérale de Lausanne, 1015 Lausanne, Switzerland

Received 7 January 2014; received in revised form 10 June 2014; accepted 11 July 2014
Available online 16 August 2014

Abstract

The gold–indium system is of primary interest for bonding processes such as solid–liquid interdiffusion bonding. In order to optimize the manufacturing parameters, it is essential to know which intermetallic compounds (IMCs) are formed when solid Au and liquid In are brought into close contact with each other, and what are their growth kinetics. For this purpose, we fabricated diffusion couples above and below the melting point of In (for $T = 250$ and 150 °C respectively). Three IMCs, identified as $AuIn_2$, AuIn and Au_7In_3, are always observed in the reaction zone, even after short times. $AuIn_2$ is the thickest and fastest growing layer and AuIn is only present as a thin layer. Whereas $AuIn_2$ and AuIn exhibit an equiaxed structure, Au_7In_3 is found to grow as columnar grains. The diffusion coefficients in each phase were determined by means of a 1-D finite difference modelling of In diffusion. The values are consistent and can be used to predict the growth rate as a function of temperature and time, i.e. to simulate a whole bonding process with finite thicknesses.

Keywords: Gold; Indium; Diffusion; Intermetallic compounds growth

1. Introduction

Microelectromechanical systems (MEMS) devices must be fabricated in a way that allows them to subsequently become parts of more complex structures without being damaged during the assembly steps. Several bonding steps occur throughout the whole process and, during each of them, the integrity of the previous bond must be preserved. Solid–liquid interdiffusion (SLID) bonding is thus an advantageous way of achieving hermetic packaging for MEMS devices [1,2]. The process consists in bringing together two metallic layers with respectively high and low melting points. By heating the system to a temperature above the lowest melting point, one or more solid intermetallic compounds (IMCs) form by interdiffusion, their melting temperature usually being between those of the two initial materials. Bonds can thus be made at a low temperature, while allowing the MEMS to withstand higher temperatures in subsequent operations, such as its mounting on printed circuit boards. The process time and temperature depend strongly on the growth kinetics of the IMCs that are formed.

The gold–indium system was chosen in the present study because In melts at a low temperature (156.6 °C) and all the phases susceptible to forming by interdiffusion have melting points above 450 °C (see the phase diagram in Fig. 1). This system has been investigated by a few authors for temperatures below the melting point of In. Powell and

* Corresponding author at: The Swatch Group R&D S.A., division Asulab, 2074 Marin, Switzerland.
E-mail addresses: lea.deillon@gmail.com (L. Deillon), thierry.hessler@a3.epfl.ch (T. Hessler), aicha.hessler@epfl.ch (A. Hessler-Wyser), michel.rappaz@epfl.ch (M. Rappaz).
[1] Present address: Institut Jean Lamour, 54000 Nancy, France.

http://dx.doi.org/10.1016/j.actamat.2014.07.025
1359-6454/

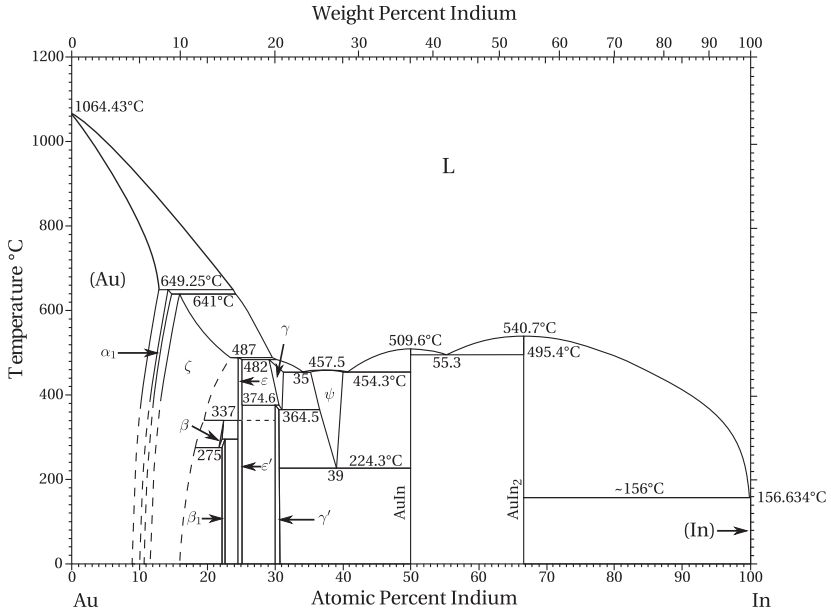

Fig. 1. The Au–In binary phase diagram [3].

Braun [4] investigated the Au–In interdiffusion at 142 and 151 °C. The major component of the reaction zone was found to be $AuIn_2$, its growth being linear with the square root of the diffusion time. Powell and Braun noticed that In is the fastest diffusing species through this compound. The IMCs Au_9In_4 (corresponding to γ' in the later version of the phase diagram shown in Fig. 1), AuIn and an Au-richer phase were also observed but as much thinner layers, and thus their growth kinetics were not studied. The Au-richer phase was very thin and was assumed to be β, since at that time this was the only known IMC with a composition lying between (Au) and γ'. A Matano analysis allowed Powell and Braun to estimate the interdiffusion coefficients in these four IMCs and the solid solutions (see Table 1).

Jellison [5] studied the growth of $AuIn_2$ between 40 and 125 °C at the interface between gold wires bounded to a nearly flat indium surface. The test was not really one-dimensional (1-D), and the presence of a free surface allowed the IMC to move out of this surface. The author noticed that the newly formed IMC appears at the surface of Au, while the earlier formed grains are carried towards In, but also upwards, inducing plastic deformation in this very soft phase. She assumed a linear relationship between the reaction time and the layer thickness, but her results, at least those at 125 °C (only three data points), actually seem to fit a parabolic law better.

Table 1
Interdiffusion coefficients and diffusion coefficients of In in the Au–In system at 151 °C ($m^2\ s^{-1}$) [4].

	$\widetilde{D}$	D
In, 3%at. Au	9.9×10^{-17}	5×10^{-15}
$AuIn_2$	1.8×10^{-15}	7.4×10^{-15}
AuIn	3.6×10^{-16}	9.1×10^{-16}
Au_7In_3 (γ')	5.8×10^{-16}	9.8×10^{-16}
β	7.8×10^{-17}	1.1×10^{-16}
Au, 9%at. In	6.2×10^{-17}	7.1×10^{-17}

Millares et al. [6] observed the growth of $AuIn_2$, AuIn, Au_7In_3 and a fourth phase, assumed to be Au_4In, in diffusion couples between 50 and 150 °C. $AuIn_2$ was found to also be the major IMC with an equiaxed grain morphology, while Au_7In_3 had a columnar structure. These authors studied the growth kinetics of $AuIn_2$ only and found a linear relationship between thickness and time in the first stage (i.e. controlled by an interfacial reaction), which then tends to become parabolic as the thickness increases.

Liu and Chuang [7] analyzed the morphology and the growth kinetics of $AuIn_2$ between 225 and 350 °C. They observed this IMC as a continuous wavy crystalline layer and as floating islands in the In phase, and reported that the growth of the layer followed a parabolic law. To our knowledge, this is the only study of the growth of IMC in the Au–In system above the melting point of indium.

Whereas data about the growth kinetics of $AuIn_2$ in the temperature range suitable for a SLID process are available, there are none for the growth of other IMCs. Furthermore, there are even some discrepancies about the number of IMCs that form under certain conditions. The aim of the present work is thus to study the growth of each IMC formed below and above the melting point of indium. From these data, the diffusion coefficients within the various phases will be determined with the help of a specifically developed 1-D finite difference numerical model of diffusion coupled with thermodynamic data.

2. Experimental

Au/In diffusion couples below and above the melting point of In (for $T = 150$ and 250 °C respectively) were fabricated in order to measure the IMCs thicknesses as a

function of time and temperature. The experiments at 250 °C were made by dipping a gold wire into liquid In melted from shot with a purity of 99.9999 wt.%, under 800 mbar of Ar. The In bath was first saturated with Au and homogenized to minimize the dissolution of the wire. After times ranging from 225 to 625 s, the wires were removed from the crucible and rapidly cooled down with a helium flux. The maximum dipping time at this temperature was limited due to experimental difficulties associated with large density differences, as discussed later.

The same setup was used for the experiments at 150 °C but after immersion of the wire, the indium bath was rapidly cooled down and solidified around the wire. In this case, the indium bath was not pre-saturated with gold since the solubility of Au in liquid In is almost nil just above the melting point. A transverse slice of the ingot and wire was then sealed in a quartz capsule under 300 mbar Ar and heat-treated in the solid state for various times ranging from 1 to 484 h. The reaction times are much longer in this case because diffusion is slower than at 250 °C.

Au wires of 99.9985 wt.% purity with a diameter of 1 mm were used for experiments longer than 81 h at 150 °C while wires of 99.998 wt.% purity and 100 μm in diameter were used for all the other cases. The obtained samples were finally cold mounted in epoxy and transverse sections were surfaced with an ultramicrotome before being analyzed using scanning electron microscopy (SEM) and backscattered electron (BSE) imaging. Energy dispersive X-ray (EDX) analyses were performed to determine the nature of the IMCs.

Additionally, secondary ion mass spectrometry (SIMS) depth profile analyses were carried out in order to measure the In concentration profiles in Au. A dynamic SIMS (DSIMS) analysis was performed by CAMECA with an IMS 7f instrument using Cs^+ primary ions at 5 keV impact energy. A time-of-flight (ToF)-SIMS analysis was also performed by Tascon GmbH using Cs^+ ions at 1 keV for sputtering and Bi_x^+ ions at 25 keV for analysis.

3. Results

3.1. Morphology of the reaction zone

3.1.1. Experiments at 150 °C

At 150 °C three IMCs are always observed in the interdiffusion zone and were identified by EDX measurements as $AuIn_2$, AuIn and Au_7In_3 (γ'). Scanning electron micrographs after various times of reaction at this temperature are shown in Fig. 2 with a brightness level directly proportional to the Au concentration (BSE contrast). Starting from indium on the right, a first layer of $AuIn_2$ is observed; it is obviously the most important IMC formed during the reaction. It has a very irregular shape, forming a loose microstructure of blocky grains, with some In channels in between. The mid-layer consists of AuIn, which grows very slowly and is observed to be thin (maximum thickness of 3.6 μm after 484 h). The third IMC, Au_7In_3, grows more regularly and its interface with Au remains almost planar, even after prolonged reaction times. Some porosity is always present locally in this compound, although this is not obvious on the SEM micrographs presented in Fig. 2, especially for the longest times, because of the lower magnifications. The voids are moreover aligned in a plane located near the Au interface. It is also noticeable that, for short reaction times, the Au_7In_3/AuIn and AuIn/$AuIn_2$ interfaces follow the irregularities of the $AuIn_2$/In interface to some extent.

The $AuIn_2$ microstructure at long reaction times (Fig. 2 right, 484 h) looks more compact than at shorter times (Fig. 2 left and middle, 1 and 64 h, respectively). However, it should be kept in mind that, for the longest reaction times (greater than 81 h), the diameter of the Au wire was 1 mm instead of 100 μm. However, with the grain size and surface finish of the two types of wires being identical, the difference in the $AuIn_2$ morphologies probably does not arise from that. Note also that the $AuIn_2$ grain size increases with time and is up to several tens of micrometers after 484 h.

Fig. 3 shows SEM micrographs of a sample treated for 324 h at 150 °C, taken with a low-angle backscattered electrons (LABE) detector. This imaging mode yields a crystallographic contrast, provided the sample has a good quality surface. Due to the inherent softness of both Au and In, this could only be achieved by cross-section polishing. The grain structure of the different phases is clearly visible on these micrographs. Gold has a very fine grain structure ($d_{eq} = 0.8 \pm 0.3$ μm), as expected for drawn wires. The growth of Au_7In_3 is columnar, with an average grain width of a few microns (3.9±1.1 μm). The AuIn grain size is small ($d_{eq} = 2.1 \pm 0.75$ μm) and is at most equal to the layer thickness. Actually, it seems to be a monolayer of grains, except in the upper parts of pictures (a) and (b), where the layer is much thicker. Concerning $AuIn_2$, smaller grains are observed near the interfaces, with larger grains in the middle of the layer. The average grain size throughout the layer is 14.6±3.4 μm.

As will be shown later (see Fig. 8), the initial gold–indium interface is positioned in the $AuIn_2$ compound, at a mean distance of 1 and 10 μm from the $AuIn_2$/AuIn interface after 144 and 225 h, respectively.

3.1.2. Experiments at 250 °C

At 250 °C the same three IMCs are observed, even after short reaction times (Fig. 4). The saturation of the In bath over a long time period is difficult due to the large difference between the Au and In densities ($\rho_{Au} = 19.3$ and $\rho_{In} = 7.3$ g/cm^3). Thus, convection movements cannot be avoided and $AuIn_2$ grains, which are not very compact and heavier than In, have a tendency to detach from the wire and deposit at the bottom of the crucible. An additional experiment with a reaction time of 7 h was also performed with an alternative setup, the saturated liquid In in this case being poured onto a gold plate. The ψ phase, which is not stable below 224.3 °C (Fig. 1), is present in this sample as a thin layer between Au_7In_3 and AuIn

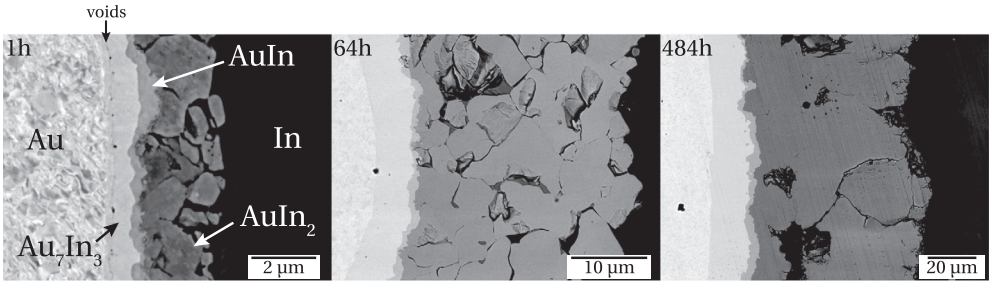

Fig. 2. SEM/BSE micrographs of IMCs after reaction at 150 °C for 1 (left), 64 (center) and 484 h (right). Gold (left) and indium (right) are separated from left to right by distinct layers of Au_7In_3, AuIn and $AuIn_2$.

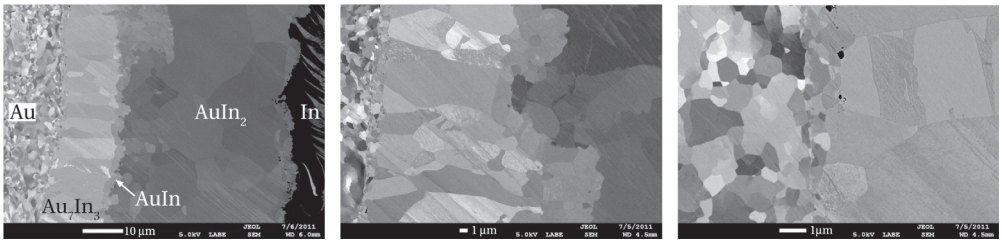

(a) general view (b) Au_7In_3 and AuIn (c) Au / Au_7In_3 interface

Fig. 3. SEM/LABE micrographs of the sample treated for 324 h at 150 °C showing crystallographic contrast; Au_7In_3 growth is columnar whereas the growth of AuIn and $AuIn_2$ is equiaxed.

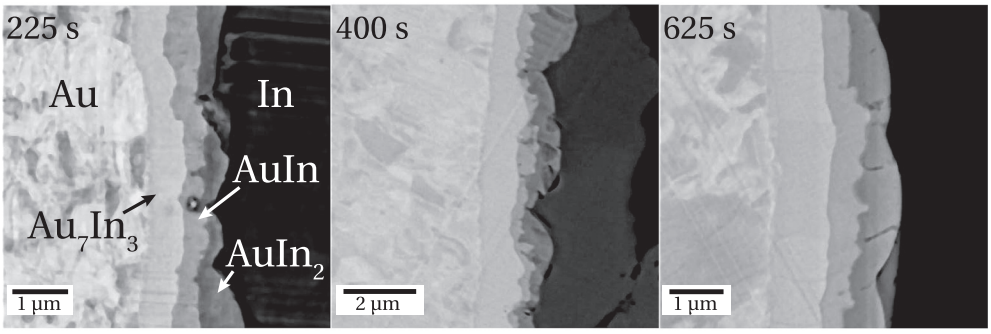

Fig. 4. SEM/BSE micrographs of IMCs growing at 250 °C. Gold (left) and indium (right) are separated from left to right by distinct layers of Au_7In_3, AuIn and $AuIn_2$.

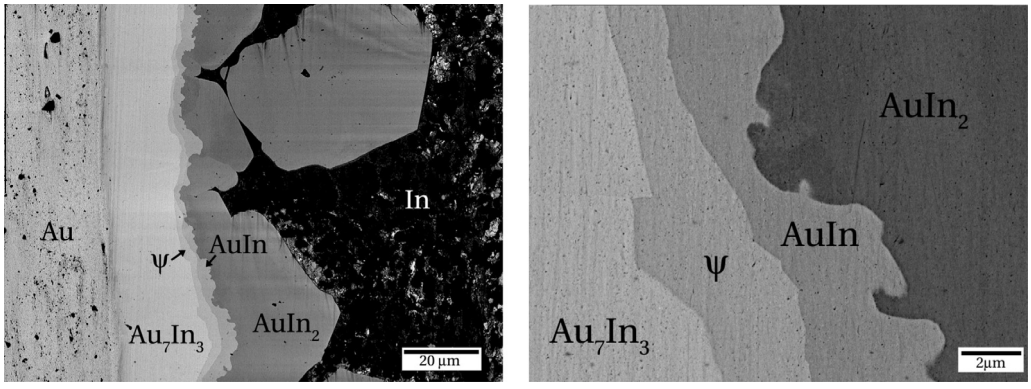

Fig. 5. SEM/BSE micrographs after 7 h at 250 °C with a horizontal configuration where the saturated liquid indium is poured onto gold: general view (left) and detailed view (right). From left to right: Au_7In_3, ψ, AuIn and $AuIn_2$.

(Fig. 5). To our knowledge, this is the first time that the ψ phase has been observed in an Au–In diffusion couple.

3.2. Growth kinetics

The average thicknesses of the three IMCs were measured on several SEM micrographs along the interface for each diffusion time and temperature. The measurements were done based on the different grey levels coming from the BSE contrast. Given the observed growth irregularities, especially for the $AuIn_2$ layer, care was taken to perform sufficient measurements in order to obtain representative values.

For both temperatures, the IMCs thicknesses (Δx) are plotted as a function of the square root of the reaction time in Fig. 6, where the error bars correspond to the standard deviations of the measurements. As can be seen, the expected parabolic law is well respected for all the IMCs at 150 °C (left figure): least-squares fits of these data with a power-law function at^n give $n = 0.53, 0.44$ and 0.53 for Au_7In_3, AuIn, and $AuIn_2$ respectively. These fits almost correspond to the parabolic fits drawn as dashed lines in Fig. 6 (left). We can further observe that the irregular aspect of $AuIn_2$ induces more scattering in the data.

At 250 °C, the measured thicknesses of $AuIn_2$ are very likely underestimated at short reaction times due to the detachment and sedimentation of the grains (see the enlarged view shown in the inset of Fig. 6, right). The least-squares fit exponents n at this temperature are 0.48 for AuIn and 0.78 for Au_7In_3. The latter value does not agree with a parabolic growth law and thus does not correspond to the straight line shown in Fig. 6 (right). Note that the measured thicknesses of Au_7In_3 are too small at short times, but the differences with a parabolic fit (straight lines) are only 1–2 μm.

The growth constants ($K = \Delta x^2/t$) in Fig. 6 for each IMC are listed in Table 2. The growth constant of $AuIn_2$ at 250 °C is close to the value found by Liu and Chuang [7] with initially pure In (3×10^{-14} m^2 s^{-1}), despite the fact that it was calculated only from the thickness measured after 7 h.

Table 2
Growth constants K [m^2 s^{-1}] of IMCs formed at 150 °C and 250 °C.

	150 °C	250 °C
Au_7In_3	$1.7 \pm 0.1 \times 10^{-16}$	$1.3 \pm 0.2 \times 10^{-14}$
AuIn	$9.8 \pm 1.6 \times 10^{-18}$	$2.45 \pm 0.1 \times 10^{-16}$
$AuIn_2$	$2.3 \pm 0.2 \times 10^{-15}$	5.5×10^{-14}

3.3. Diffusion profiles in Au

Fig. 7 shows the results of SIMS depth profiles measured in gold for two samples heat-treated for 484 h at 150 °C (left) and for 7 h at 250 °C (right). The experimental data were fitted with the exact analytical solution of the diffusion equation assuming a constant concentration C^*_{Au} at a motionless interface, with the boundary conditions $C(x, t = 0) = 0$ and $C(\infty, t) = 0$:

$$C(x,t) = C^*_{Au}\mathrm{erfc}\left(\frac{x}{2\sqrt{D^{Au}t}}\right) \quad (1)$$

where erfc is the complementary error function, D^{Au} is the diffusion coefficient of In in Au and C^*_{Au} is the concentration of In in Au at the interface with Au_7In_3. Since these SIMS measurements were made on inclined sections in order to limit the sputtering time, the bevel angles had to be accounted for in the deconvolution of the results. In contrast, the cylindrical geometry of the first sample was ignored, the size of the analyzed area ($\sim 50 \times 50$ μm^2) being small compared to the wire radius (0.5 mm). The fits give a value of D^{Au} at 150 °C of 10^{-18} m^2 s^{-1}, i.e. a value about 0.15 times that found by Powell and Braun [4], while at 250 °C $D^{Au} = 2 \times 10^{-17}$ m^2 s^{-1}.

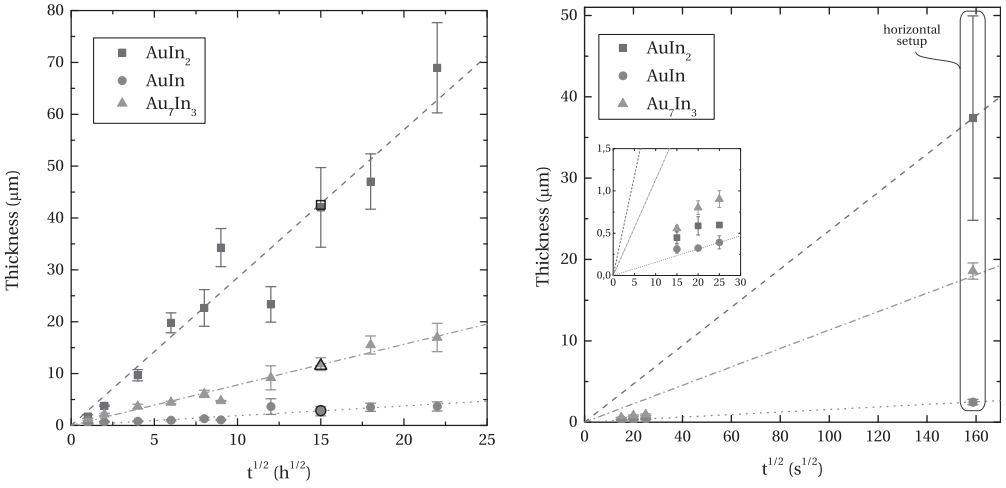

Fig. 6. IMCs growth: measured thickness vs square root of the diffusion time at 150 °C (left) and 250 °C (right). Filled squares, circles and triangles correspond to the measured thicknesses of $AuIn_2$, AuIn and Au_7In_3, respectively, while the open symbols after 225 h of reaction in the left figure correspond to the simulation shown in Fig. 8 (right).

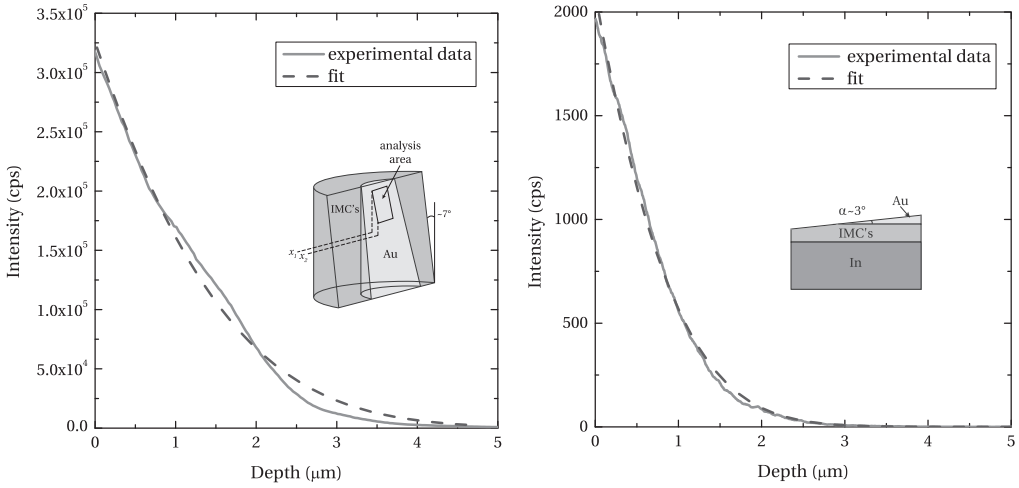

Fig. 7. Indium profiles in Au: experimental data and fits with Eq. (1), taking into account the inclined section. Left: 484 h at 150 °C (DSIMS); right: 7 h at 250 °C (ToF-SIMS).

4. Modeling of IMCs growth

4.1. FDM model

The diffusion couples being supposed to be isothermal, the growth of the various IMCs is governed by solute diffusion, and possibly interface kinetics if their velocities are high. A numerical model was developed to solve the diffusion equations in the various phases, i.e. Au and the three IMCs, in order to reproduce the growth of the IMCs. The main assumptions of the model are: (i) diffusion of In is supposed to occur much faster than the diffusion of Au; (ii) no consideration of the nucleation stage of the IMCs; (iii) local equilibrium at the interfaces (i.e. no interface kinetics contribution); (iv) liquid indium initially saturated with gold; and (v) linear variation of the chemical potential across each IMC, given by the difference of the equilibrium chemical potentials with the neighboring phases on each side of the IMC, divided by its thickness.

The diffusion of In into the Au phase was computed using a front-tracking 1-D numerical model to solve Fick's second law in the moving reference frame $x \in [0, x^*(t)]$, after a Landau transformation into a fixed reference frame $\eta(x,t) = x/x^*(t) \in [0,1]$, where x^* is the position of the Au/Au_7In_3 interface (see Ref. [9]). The diffusion equation of In in the Au phase then becomes:

$$\left(\frac{\partial C}{\partial t}\right)_x = \left(\frac{\partial C}{\partial t}\right)_\eta - \frac{v^*\eta}{x^*}\left(\frac{\partial C}{\partial \eta}\right)_t = \frac{1}{x^{*2}}\frac{\partial}{\partial \eta}\left(D^{Au}\frac{\partial C}{\partial \eta}\right)_t \quad (2)$$

where $C(x,t)$ is the In concentration (in at m^{-3}), D^{Au} is the diffusion coefficient of In in Au and v^* is the velocity of the Au/Au_7In_3 interface. Note the appearance of an advection term associated with the movement of the Au/Au_7In_3 interface. This equation was solved numerically with a fixed interval and number of mesh points using an explicit scheme and a Neumann boundary condition in $x = 0$. For the mesh point "i", the equation to be solved in the gold phase becomes:

$$\frac{C_i^{t+\Delta t} - C_i^t}{\Delta t} = D^{Au}\frac{C_{i+1} - 2C_i + C_{i-1}}{(x^* \times \Delta\eta)^2} + \frac{v^* \times (i-1) \times \Delta\eta}{x^*} \times \frac{(C_{i+1} - C_{i-1})}{2\Delta\eta} \quad (3)$$

The flux of indium in gold at the Au/Au_7In_3 interface was then calculated as:

$$J^{Au} = -D^{Au}\frac{C_2 - C_1}{\Delta\eta \times x^*} \quad (4)$$

The In fluxes in the IMCs were calculated from chemical potential gradients since these phases are stoichiometric. The IMCs possess very sharp free energy curves; consequently, a very slight change in composition results in a large variation of the chemical potential. The atomic flux in the IMC α in that case is given by:

$$J^\alpha = -M^\alpha C^\alpha \frac{\Delta\mu^\alpha}{\Delta x^\alpha} \quad (5)$$

where M^α is the atomic mobility of In in the IMC α, C^α is its (stoechiometric) composition and $\Delta\mu^\alpha$ is the chemical potential difference across its thickness Δx^α. In order to make the discussion and comparisons easier, the atomic mobilities M^α were converted into equivalent diffusion coefficients, D^α, assuming that the IMCs can be treated as regular solutions, using the following relationship:

$$D^\alpha = M^\alpha RT\left(1 - \frac{2\Delta H^\alpha_{mix}}{RT}\right) \quad (6)$$

where R is the gas constant, T is the temperature and ΔH^α_{mix} is the enthalpy of mixing (values taken from Ref. [8]). The velocity of an α–β interface, $v_{\alpha\beta}$, is finally obtained by the application of mass and solute conservation equations (see Ref. [10]):

$$(\rho^{\beta} - \rho^{\alpha})v_{\alpha\beta} = \rho^{\beta}v_{\beta} - \rho^{\alpha}v_{\alpha} \quad (7)$$

$$\rho^{\beta}C^{*}_{\beta}(v_{\beta} - v_{\alpha\beta}) - \rho^{\alpha}C^{*}_{\alpha}(v_{\alpha} - v_{\alpha\beta}) = j^{\alpha *} - j^{\beta *} \quad (8)$$

where ρ^{v} and v_{v} are the density and velocity in the phase v, respectively, while C^{*}_{v} and j^{v*} are the interfacial concentration and mass flux at the interface position in the phase v. The density differences are taken into account, thus allowing one to predict the evolution of the overall size of the system, which is an important parameter for a finite domain such as that encountered in SLID bonding. The equations were solved assuming the velocity in gold, v_{Au}, to be zero.

The starting configuration was made of 60 μm of gold and 80 μm of saturated indium separated by thin layers (0.05 μm) of Au_7In_3, AuIn and $AuIn_2$. The initial mesh size in the Au phase was set to 60 nm, with 1000 mesh points. The results were shown to be independent of the mesh size as the growth constants were found to be identical with an initial mesh size of 4 nm. Thermodynamic data were computed based on the work of Liu et al. [8].

4.2. Optimization of the diffusion coefficients

The diffusion coefficients were adjusted to reproduce the growth constants obtained experimentally. In addition to the evolution of the IMC thicknesses, their position with respect to the initial gold–indium interface position was used as an additional parameter to be fitted by the simulation. This then gives the same number of parameters to be fitted (i.e. the four diffusion coefficients in the three IMCs and gold, indium being saturated) as the number of observable entities (three IMC thicknesses and a reference position).

As an example, Fig. 8 (left) shows an SEM/BSE micrograph of a sample maintained for 225 h at 150 °C, for which the gold wire surface was partially protected by the application of an epoxy enamel (Berlapoxy™) before its immersion in the indium bath. The original Au/In interface is extended in the reaction zone by the dashed white circle. As already stated in the previous section, the initial Au/In interface is located in the $AuIn_2$ compound, at a mean distance of about 10 μm from the $AuIn_2$/AuIn interface after 225 h. The corresponding simulated growth of IMCs at 150 °C is shown on the right of Fig. 8 as a function of time. The original interface is shown with a dashed black line, and its position with respect to the $AuIn_2$/AuIn interface corresponds fairly well to the observation on the left. The predicted thicknesses of the various IMCs after 225 h at 150 °C are 42.5, 2.8 and 11.5 μm for $AuIn_2$, AuIn and Au_7In_3, respectively. These values, shown with open symbols in Fig. 6 (left), agree very well with the parabolic law fitted to the experimental data.

Diffusion being a thermally activated process, the diffusion coefficients can be expressed as a function of temperature using an Arrhenius equation:

$$D(T) = D_0 \exp\left(-\frac{E_a}{RT}\right) \quad (9)$$

The pre-exponential factors D_0 and activation energies E_a for the diffusion of In in the different phases are listed in Table 3. It is notable that the activation energy for the diffusion across Au_7In_3 is larger than that for diffusion across the other phases. Errors on D are estimated from the errors on the experimental growth constants and thus no error is given for the diffusion coefficient in the gold phase. The estimated errors on the pre-exponential factors are large, as they are computed from extremal values of $\ln(D_0)$.

5. Discussion

5.1. Porosity formation

Microporosity was observed near the Au/Au_7In_3 interface, in the Au_7In_3 phase. It has a very small size (typically on the order of 0.15 μm) and is intragranular. A few such pores are visible in the middle of Fig. 3(c) and in Fig. 9(a). By serial sectioning using a focused ion beam (FIB), it was observed that this microporosity is located in a plane more or less parallel to the Au/Au_7In_3 interface (Fig. 9(b)). At 150 °C, the distance δ_p of this porosity "plane" to the Au/Au_7In_3 interface also increases with

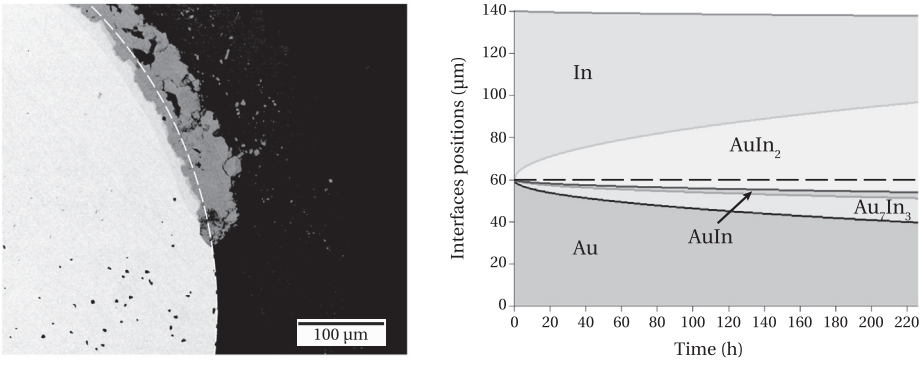

Fig. 8. Left: SEM/BSE micrograph after 225 h at 150 °C; the initial Au/In interface was marked prior to experiment and its position is represented by the dashed white line. Right: IMC growth simulated at the same temperature; the dashed black line indicates the original Au/In interface.

Table 3
Pre-exponential factors D_0 and activation energies E_a for In diffusion.

	D_0 [m^2 s^{-1}]			E_a [kJ/mol]		
$AuIn_2$	5.2×10^{-8}	+	6.1×10^{-8}	61.3	+	3.0
		−	3.1×10^{-8}		−	3.4
AuIn	3.1×10^{-9}	+	1.5×10^{-9}	57.5	+	1.1
		−	1.0×10^{-9}		−	1.0
Au_7In_3	4.05×10^{-7}	+	8.15×10^{-7}	72.0	+	3.7
		−	2.85×10^{-7}		−	4.1
Au	6.9×10^{-10}			64.5		

the square root of the diffusion time, following the law: $\delta_p(t)[\mu m] = 1.67\times10^{-3}t^{1/2}[s]$. The size and location of this microporosity indicate that it probably results from a Kirkendall effect, and not from a density difference ($\rho_{Au_7In_3} < \rho_{Au}$). However, it is difficult to assess the importance of this effect in the present case for at least two reasons: (i) a flux of vacancies due to a difference between the diffusion coefficients of Au and In can indeed lead to the formation of microporosity if the vacancies condense into micropores, but the vacancies can also modify the absolute position of the interfaces if they can be annihilated (e.g. by dislocation climb). Therefore, the absolute position of an interface, which depends on the change in density (accounted for in the present investigation), is also linked to the Kirkendall effect (ignored here); and (ii) there are three IMCs involved in addition to the Au and In phases, and thus four interfaces with only one known absolute reference position, namely the initial position of the Au/In interface. This reference position has already been used in the estimation of the diffusion coefficients and mobilities, and thus cannot provide additional information on the Kirkendall effect.

5.2. Diffusion and growth

Except for the indium phase, the two temperatures at which the diffusion couple experiments were made are lower than 3/4 of the melting point of the observed phases (in K). Therefore, diffusion is expected to occur mainly along grain boundaries [11]. According to the studies mentioned above, $AuIn_2$ grows mainly by diffusion of In atoms and reaction at the interface with AuIn. If the diffusion of Au atoms is much slower, this results in a net flux of vacancies in the opposite direction (Kirkendall effect).

Diffusion along Au_7In_3 grain boundaries is made easier thanks to its columnar structure. The presence and location of porosity suggest that the diffusion of Au atoms through Au_7In_3 is faster than the diffusion of In. A schematic of the diffusion across the various phases is shown in Fig. 10. It appears that AuIn acts as a barrier for both In diffusing to the left and Au diffusing to the right. This phenomenon is reflected in both the very low growth rate of this IMC (Table 2) and and the low In diffusion coefficient (Table 3).

The modelling assumption that In can be considered as the only diffusing species does not seem to hold for Au_7In_3. Consequently, the estimated diffusion coefficients of In through this IMC are most likely overestimated, the values including also diffusion of Au atoms.

The diffusion coefficients of In in gold predicted by the model on the basis of the IMC growth kinetics can be compared with the SIMS experimental results. At 150 °C, the SIMS analyses provide a value of D^{Au} equal to 10^{-18} m^2 s^{-1}. By means of the numerical model, we determine a value three times lower: $D^{Au} = 3\times10^{-19}$ m^2 s^{-1}. However, there is a lack of accuracy concerning this experimental result

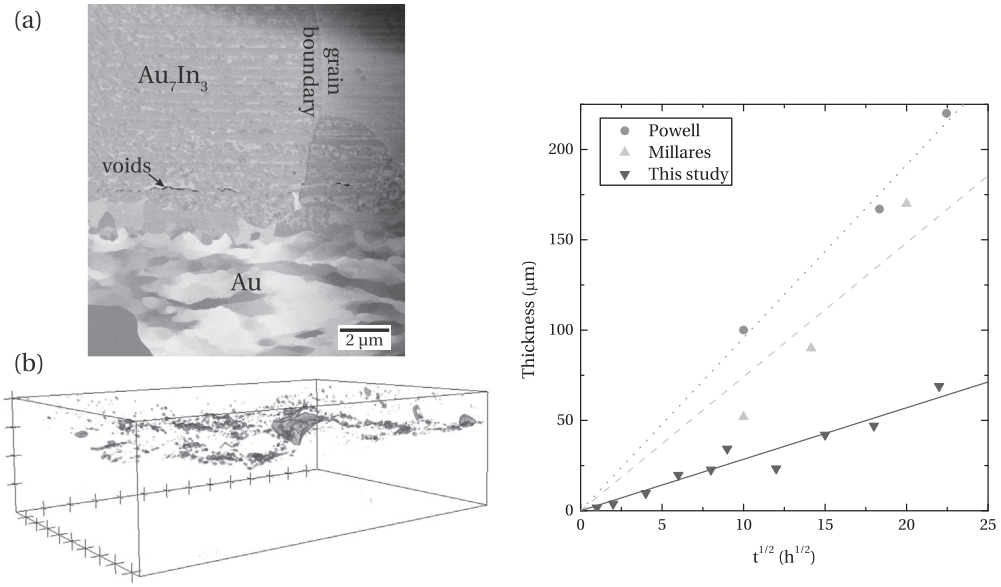

Fig. 9. Left: (a) location of the porosity observed in Au_7In_3 at 250 °C after 7 h (SEM/energy selective backscattered) and (b) 3-D reconstruction of this porosity using a FIB. The graduation in (b) corresponds to 1 μm and the Au/Au_7In_3 interface is below the porosity in both figures. Right: comparison of the results obtained for $AuIn_2$ and those reported in the literature [4,6].

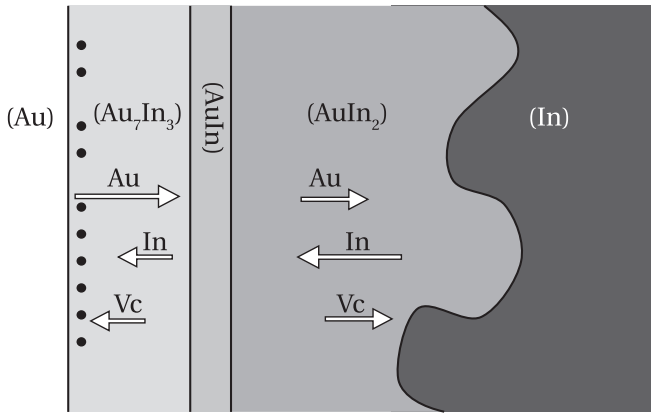

Fig. 10. Schematic of Au, In and vacancy diffusion in the Au–In system.

and, consequently, we did not use it to fit the value implemented in the model. At 250 °C, fitting the SIMS data gives $D^{Au} = 2 \times 10^{-17}$ m^2 s^{-1}, while an adjustment of the parameters of the model predicts a value about half of that ($D^{Au} = 8 \times 10^{-18}$ m^2 s^{-1}).

The diffusion coefficients at 150 °C can also be compared to the results from Powell and Braun [4]. These authors determined values of $\tilde{D}$ from a Matano analysis assuming a homogeneity range of 10 at.% for each IMC. The method then used to extract the diffusion coefficients of In is, however, not explained. In the IMCs, these values of D are slightly larger than the values obtained in the present study. The difference is more important in gold, where an order of magnitude separates the values. We noted that our results are actually closer to the values of $\tilde{D}$ from Powell and Braun.

The influence of the Au microstructure on In diffusion, and thus on IMCs growth, is not part of this study since the Au substrates used are not significantly different in terms of grain size. However, the diffusion of In in Au is very limited and the microstructure of Au_7In_3 is not related to the Au microstructure. Consequently, the IMC growth seems to be mainly controlled by the diffusion through them. The simulations confirm this result as they give growth constants that are not very sensitive to the choice of D_{Au}.

5.3. Comparison of $AuIn_2$ growth with literature data

There is no study available in the literature concerning the growth of AuIn and Au_7In_3, but the growth kinetics of $AuIn_2$ determined in the present work can be compared with former studies (Fig. 9, right). At 150 °C, the kinetics obtained in the present study is slower than the kinetics previously reported. This discrepancy might come from a larger $AuIn_2$ grain structure which can slow down the diffusion process. With an average size approaching 15 μm after 324 h, the observed $AuIn_2$ grains are substantially larger than in other studies. Millares et al. [6], for example, reported a grain size of 2–4 μm independent of diffusion time, whereas they measured a grain size similar to our results for the other IMCs. In the present study, it seems that the $AuIn_2$ grains are smaller in the experiments conducted with the 100 μm diameter gold wires, and this IMC is also less compact in this case. While coarsening of the grains may occur, it is probably not the reason for this discrepancy and we do not have any explanation for the differences in $AuIn_2$ microstructures.

6. Conclusion

A number of conclusions can be drawn from the Au–In diffusion couples experiments:

- $AuIn_2$, AuIn and Au_7In_3 are the three IMCs that are always observed at 150 and 250 °C regardless of the diffusion time. Their growth was shown to follow the expected parabolic law at both temperatures. $AuIn_2$ forms the majority of the reaction zone and grows irregularly, forming blocky grains. Au_7In_3 is the second IMC in terms of thickness and grows much more regularly, with a nearly flat interface with Au. AuIn was only observed as a thin layer and seems to act to some extent as a diffusion barrier for both In and Au.
- At 250 °C, an additional thin layer of ψ is also present after 7 h when a horizontal configuration of the diffusion couple is adopted.
- SEM observations with a LABE detector allowed us to visualize the microstructure of the IMCs: Au_7In_3 grows in a columnar way, whereas both $AuIn_2$ and AuIn have an equiaxed grain morphology.
- Au atoms appear to diffuse much faster than In through Au_7In_3. This conclusion is based on the observed porosity, which probably results from a Kirkendall effect.
- The diffusion of In in Au is very slow and the growth of the IMCs seems to be mainly controlled by the diffusion through them.

The main results and limitations of the 1-D numerical model developed can be summarized as follows:

- The model reproduces the observed experimental growth well and provides values of the indium diffusion coefficients that are of reasonable orders of magnitude.
- The model tends to confirm that the growth of the IMCs is mainly controlled by the diffusion through them as their growth is not significantly affected by the value used for the diffusion coefficient of In in Au.
- As the model is monodimensional, the growth instabilities are not taken into account. This does not represent a major limitation for Au_7In_3 and AuIn since their growth is rather regular. By contrast, $AuIn_2$ was shown to grow irregularly and the description of this IMC is thus more limited: only the evolution of its average thickness can be reproduced.
- The assumption was made that we could ignore the diffusion of Au and only consider the diffusion of In, which is apparently not true for Au_7In_3. The obtained diffusion coefficients are effective diffusion coefficients which take into account the different contributions to diffusion.

Acknowledgments

The Swatch Group R&D S.A., division Asulab, is gratefully acknowledged for funding this work. The authors also thank JEOL for the CSP polishing and LABE imaging, and CAMECA for the DSIMS analyses.

References

[1] Bernstein L. J Electrochem Soc 1966;113:1282.
[2] Bernstein L, Bartholomew H. Trans Metall Soc AIME 1966;236:405.
[3] Okamoto H, Massalski T. Binary alloy phase diagrams. 2nd ed. Metals Park, OH: ASM; 1990.
[4] Powell GW, Braun JD. Trans Metall Soc AIME 1964;230:694.
[5] Jellison JE. Technical Report NASA GSFC Code 313. Materials Control and Applications Branch; 1979.
[6] Millares M, Pieraggi B, Lelievre E. Solid State Ion 1993;63–65:575.
[7] Liu Y, Chuang T. J Electron Mater 2000;29:405.
[8] Liu HS, Cui Y, Ishida K, Jin ZP. CALPHAD 2003;27:27.
[9] Rappaz M, Bellet M, Deville M. Traité des matériaux. Modélisation numérique en science et génie des matériaux, vol. 10. Lausanne: Presses Polytechniques et Universitaires Romandes; 1998.
[10] Dantzig JA, Rappaz M. Solidification. Lausanne: EPFL Press; 2009.
[11] Philibert J. Diffusion et transport de matière dans les solides. Les Ulis: Ed. de Physique; 1990.